THE JOURNAL OF PHYSICAL CHEMISTRY C
A JOURNAL OF THE AMERICAN CHEMICAL SOCIETY

pubs.acs.org/JPCC

Article

Effects of Vacancy and Ti Doping in 2D Janus MoSSe on Photocatalysis

Yi-Ming Zhao, Pengju Ren, Xing-Yu Ma, James P. Lewis,* Qing-Bo Yan,* and Gang Su*

Cite This: *J. Phys. Chem. C* 2021, 125, 11939–11949

Read Online

ACCESS | Metrics & More | Article Recommendations | Supporting Information

ABSTRACT: Two-dimensional (2D) Janus transitional-metal dichalcogenides (TMDCs) have great potential for photocatalytic water splitting due to their novel properties induced by the unique out-of-plane asymmetric structures. Here, we systematically investigate the geometric, electronic, and optical properties of 2D Janus MoSSe with titanium doping and vacancies to explore their synergistic effects on photocatalytic activity. We find that there is effective attraction between the substituted or adsorbed Ti atoms and S/Se vacancies. The Ti adatoms dramatically extend the light absorption range to the infrared region. The S/Se vacancies coexisting with Ti adatoms will modulate the transition of photoexcited electrons, thereby enhancing sunlight absorption. The Ti adatoms either existing alone or coexisting with vacancies introduce smaller lattice distortion compared with substituted Ti atoms, and these Ti adatoms induce smaller effective mass of charge carriers. The configuration of S vacancy coexisting with Ti adatoms on the Se surface exhibits the most significant synergistic effects and the best overall photocatalytic performance. Our work reveals the mechanisms and effects induced by doping and vacancies coexisting in 2D Janus TMDCs and also proposes a new practical strategy to improve the performance of 2D photocatalysts.

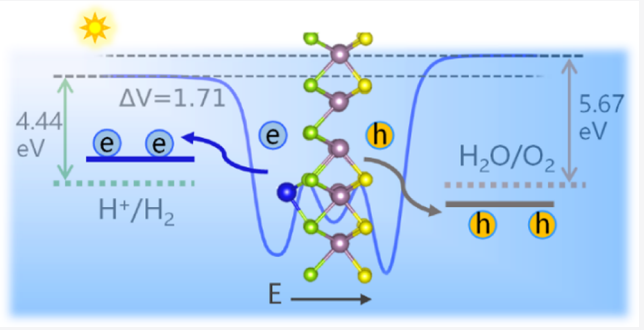

1. INTRODUCTION

Photocatalytic water splitting is a clean and renewable way to reduce the consumption of carbon-based fossil fuels and mitigate the greenhouse effect.[1] Photocatalysts such as TiO_2,[2,3] CdS,[4] Fe_2O_3,[5,6] TaON,[7] etc. can catalyze redox reactions of water splitting under sunlight; however, limited performance restricts broader applications.[8] The water-splitting reaction contains the hydrogen evolution reaction (HER) and oxygen evolution reaction (OER), as shown in Figure 1. HER referring to the reduction of H^+ ions to H_2 molecules is a crucial step for H_2 generation via water splitting. The best-performing photocatalysts should have proper band-edge energy alignments, significant carrier mobility, suitable band gaps, and proper adsorption of surface reactants.[9] The valence/conduction bands should straddle the redox reaction potentials to enable the photogenerated electrons and holes to transfer to these potentials and catalyze the redox reaction.[10] The carrier mobility determines the efficient separation of electron and hole pairs. A suitable band gap enables the semiconductors to effectively harvest sunlight energy. Finally, the proper adsorption of surface reactants will improve the efficiency of surface reactions. Two-dimensional (2D) semiconductors are promising high-performance photocatalysts due to larger specific areas for surface adsorbates to react and shorter distances for charge carriers to migrate to the surface.[11,12]

Among 2D semiconductors, monolayer molybdenum disulfide (MoS_2) exhibits potential as a material for photovoltaic and photocatalytic applications because of its proper band edges for catalyzing the water-splitting reaction,[13,14] greater mobility of charge carriers compared with many

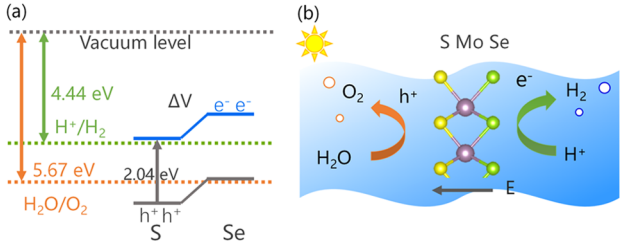

Figure 1. (a) Schematic illustration of the band edges of 2D Janus-MoSSe with respect to the redox potential of the water-splitting reaction and the bending of energy levels induced by the internal electric field. (b) Distribution of photogenerated electrons and holes and the schematic diagram of HER and OER reactions.

Received: March 3, 2021
Revised: April 20, 2021
Published: May 27, 2021

semiconductors,[15] and a direct band gap of 1.73 eV, which is in the visible range.[14,16] However, perfect MoS_2 has disadvantages such as lacking catalytically active sites due to its very smooth surface morphology. Additionally, the fast recombination of photogenerated electron−hole pairs, while excellent photoluminescence, diminishes opportunities for the absorption energy of MoS_2 to be utilized in chemical reactions.[17,18]

2D Janus materials mainly include transitional-metal dichalcogenides (TMDCs),[19,20] transition-metal trichalcogenides,[21] group-III chalcogenide monolayers,[22] Janus 2D van der Waals heterostructures,[23] etc. These Janus structures with a broken mirror or inversion symmetry are promising for the application of piezoelectric materials,[24,25] spintronics,[21] and photocatalysts.[26] Recently, Lu et al. synthesized a novel 2D Janus MoSSe (2D J-MoSSe) successfully by completely replacing all sulfur atoms on one surface of the 1H-phase MoS_2 monolayer with selenium atoms via chemical vapor deposition (CVD).[27] The 2D J-MoSSe obtains an breaking out-of-plane symmetry as the differences between S and Se, such as electronegativity, atomic radius, etc. This breaking out-of-plane symmetry induces an intrinsic internal electric field in 2D J-MoSSe, pointing from the Se plane to the S plane and perpendicular to the surface.[28] More negative charge accumulates around the S atom compared with that around the Se atom, resulting from the larger electronegativity of sulfur than that of selenium.[29] The internal electric field will boost the separation of charge carriers as well. A direct optical band gap of 1.68 eV enables 2D J-MoSSe to slightly better utilize sunlight compared with MoS_2.[28] Guan et al. hypothesized, from density functional theory (DFT) calculations of optical absorption spectra and band-edge alignments, that 2D J-MoSSe may have significant photocatalytic performance.[30] The band-edge alignments straddle the redox potential of the water-splitting reaction with a calculated band gap of 2.04 eV, as shown in Figure 1a. The electrostatic potential difference (ΔV) induced by the broken out-of-plane symmetry will modulate the work function on different surfaces and shift the band-edge levels. From the reported theory, the band edges bend upward along the direction of the internal electric field.[31,32] The Se and S sites attract photogenerated electrons and holes, respectively, and the electrons in the conduction band (localized on the Se surface) increase in energy due to the higher electrostatic potential of the Se side compared with that of the S side. The higher-energy electrons will more readily transport to the reduction potential, thereby more readily reducing the H^+ ions to H_2, while the holes more readily transport to the oxidation potential, thereby oxidizing the H_2O molecule to O_2, as shown in Figure 1b.

The ideal catalyst should adsorb the protons within the right window of binding energies (neither too weakly nor too strongly) to catalyze the HER efficiently (for a more thorough discussion of HER, see the Supporting Information). Unfortunately, the basal planes of pristine 2D J-MoSSe have difficulty adsorbing reactants (protons and water molecules).[28] The intrinsic S or Se vacancies will adsorb protons better than the basal planes, thereby significantly improving the efficiency of HER on the surfaces of 2D J-MoSSe, as shown by both experimental and theoretical results.[28,33,34] The S or Se vacancies naturally exist on the surfaces of 2D J-MoSSe when prepared by CVD, similar to MoS_2 which contains a noticeable fraction of S vacancies when prepared by either mechanical exfoliation or CVD.[35,36]

Other Janus TMDCs like WSSe also have great potential for photocatalytic water splitting based on calculated results:[19] 2D Janus WSSe has a direct band gap of 2.13 eV, slightly larger than the 2.04 eV band gap of 2D J-MoSSe. The 2D J-MoSSe is apparently superior in photocatalytic application compared with Janus WSSe due to its more predominantly reported successful synthesis within the literature, as well as its smaller band gap and high catalytic efficiency for HER. Researchers also demonstrated that adsorbed transition metals on 2D J-MoSSe will improve the reactant adsorption as well as enlarge the optical absorption range.[37] Transition metals adsorbed on the Se (S) surface of 2D J-MoSSe will strengthen (weaken) the internal electric field.[29] Intrinsic S or Se vacancies will exist simultaneously when transition metals are adsorbed on the surfaces of 2D J-MoSSe. To our knowledge, few researchers have investigated the synergistic effects on the photocatalytic properties when vacancies and adsorbed transition metals coexist on the 2D J-MoSSe surface. Understanding synergistic effects in these materials is a valuable scientific question; the answer will provide insights into the photocatalytic activity of these imperfect 2D J-MoSSe surfaces. We also believe that exploring the interactions between different types of defects is an important scientific question for developing practical photolytic applications of codoped semiconducting surfaces.

Titanium is one of the non-noble transitional-metal elements and exhibits electronic properties ideal for heterogeneous catalysts and single-atom catalysts.[38−40] For example, Ti atoms adsorbed on reduced graphene oxide are highly catalytically active for dye-sensitized solar cells.[41] Also, Ti-atom-decorated substrates are promising for hydrogen storage.[42,43] Overall, Ti doping may uniquely improve the photocatalytic activity of 2D J-MoSSe for hydrogen generation by the water-splitting reaction. In this work, we systematically study the geometric, electronic, optical absorption, and surface adsorption properties of doped 2D J-MoSSe with intrinsic vacancies and extrinsic Ti doping. Our research contributes to a comprehensive understanding of the synergistic effects of coexisting extrinsic doping and intrinsic vacancies and also provides insights into the experimental preparation of doped 2D J-MoSSe structures for improving photocatalytic activity.

2. COMPUTATIONAL METHODOLOGY

The 1H-phase MoS_2 has a hexagonal crystal lattice with a point group of D_{3h}, in which two S atom layers sandwich the Mo atom layer. The MoS_2 structure will transform to the 2D J-MoSSe structure by completely replacing one of the two S atom layers in MoS_2 with Se atoms. Figure S1 shows the geometric structures of pristine 2D J-MoSSe and MoS_2. Ti adatoms and vacancies may migrate on the surface of 2D J-MoSSe. The study of migration barriers presents how much energy the defects need to diffuse on the surface and determines whether the defects will diffuse readily or not. Synergistic effects arise when vacancies and Ti adatoms coexist in 2D J-MoSSe. The coexisting defects we considered in our calculations include various combinations like a coexisting vacancy with an adsorbed Ti atom on a hollow or a Mo-top site of the S/Se-side surface, respectively, as represented in Figure 2. The representative examples shown are (1) the coexisting intrinsic S atomic vacancy with the adsorbed Ti atom on the hollow site of the S-side surface ($Ti_S^{ad\text{-}h}V_S$), in Figure 2a; (2) the coexisting intrinsic S atomic vacancy with the adsorbed Ti atom on the Mo-top site of the Se-side surface ($Ti_{Se}^{ad\text{-}t}V_S$), in Figure 2b; (3) the coexisting vacancy with the

https://doi.org/10.1021/acs.jpcc.1c01918
J. Phys. Chem. C 2021, 125, 11939−11949

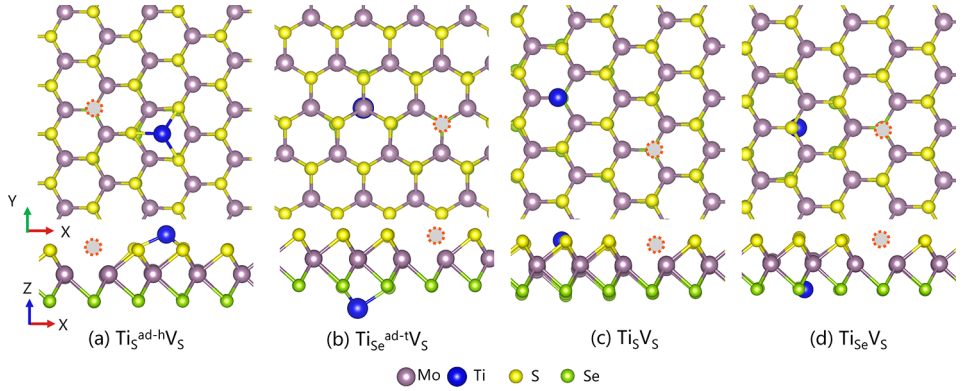

Figure 2. Schematic defect combinations in 2D J-MoSSe. (a) Top and side views of the S vacancy coexisting with the adsorbed Ti atom on the hollow site of the S-side surface ($Ti_S^{ad\text{-}h}V_S$). (b) Top and side views of the S vacancy coexisting with the adsorbed Ti atom on the Mo-top site of the Se-side surface ($Ti_{Se}^{ad\text{-}t}V_S$). (c) Top and side views of the S vacancy coexisting with the substituted Ti atom of sulfur (Ti_SV_S). (d) Top and side views of the S vacancy coexisting with the substituted Ti of selenium ($Ti_{Se}V_S$). The dashed red circles indicate the location of S vacancies. The purple, blue, yellow, and green balls represent the Mo, Ti, S, and Se atoms, respectively.

substituted Ti atom of sulfur (Ti_SV_S), in Figure 2c; and (4) the coexisting vacancy with the substituted Ti atom of selenium ($Ti_{Se}V_S$), in Figure 2d. We also consider calculations on the coexisting Se atomic vacancy with the Ti atom, as shown in Figure S2. The energetics of the various structural configurations enable us to check which configuration would likely be favorable in an experimental preparation. We first explore the variation of energy corresponding to the distance between the Ti atom and S/Se vacancy in 2D J-MoSSe (in a 9 × 9 × 1 supercell), as shown in Figure S3.

Based on the results of the lowest-energy configurations, we build simplified 4 × 4 × 1 supercells, as shown in Figure S6, to calculate the electronic properties with higher precision to investigate the photocatalytic properties. Understanding the potentiality of 2D J-MoSSe defect structures in photocatalysis, we calculate the band structure, optical absorption spectra, electrostatic potentials, effective mass, and Gibbs free energy. There are plenty of flat energy bands in the band structure of our large supercells because the band structures of a supercell get folded into the first Brillouin zone.[44] The unfolded band structure is necessary to recover an effective primitive cell band structure, thereby representing a unit cell band structure containing defect levels.[45] The transport efficiency of charge carriers is dictated by the effective mass of this unfolded band structure. The reaction barrier of HER is determined by the binding strength of H atoms at the reaction sites and the change of Gibbs free energy (also denoted by hydrogen adsorption free energy). All of these aforementioned properties are closely related to the photocatalytic activity and provide estimates of which configurations will improve the photocatalytic performance.

In our calculations, we utilize the Quantum Espresso (QE)[46] and Vienna Ab initio Simulation Package (VASP)[47] software by means of the projected augmented wave (PAW) method.[48] The neb.x routine within the QE package helps to study the migration of S and Se vacancies and the adsorbed Ti adatoms via the nudged elastic band (NEB) method.[49] The unfolded band structures of the doped supercells clearly exhibit the effects of defect states using the BandUP package.[50] We calculated the effective mass of charge carriers from the curvature of energy bands. The atomic simulation environment (ASE),[51] written in Python, enables us to submit a large number of calculations. We utilized the thermochemistry modules in ASE to efficiently calculate the hydrogen adsorption free energy and the VASPKIT[52] tools for postprocessing data generated by VASP.

3. RESULTS AND DISCUSSION

The results in our work contain migration barrier, relative energy of different configurations, and the photocatalysis-related properties of configurations with the lowest energies (optical absorption spectra, electrostatic potential difference, effective mass of charge carriers, and hydrogen adsorption free energy). Both the Ti adatom and vacancy are unable to migrate on the surface of 2D J-MoSSe, as discussed in Section 3.1. The configuration with the Ti atom adjacent to the vacancy generally has the lowest energy, as discussed in Section 3.2. In these lowest-energy configurations, the adsorbed Ti atom dramatically extends the optical absorption range of 2D J-MoSSe and the coexisting vacancy further increases the absorption coefficient, as discussed in Section 3.3. The conduction band minimum (CBM) and valence band maximum (VBM) of the defects we considered still straddle the redox potential of water-splitting reaction, as written in Section 3.4. Ti adatoms on matter existing alone or coexisting with vacancies will not greatly increase the effective mass of charge carriers, as written in Section 3.5. The hydrogen adsorption free energies on the top sites of Ti adatom are closer to zero compared with those on the top site of substituted Ti atoms, as written in Section 3.6. These results indicate that the configurations with Ti adatoms on the Se surface and S vacancy exhibit mostly improved photocatalytic activities.

3.1. Migration of Adsorbed Ti Atoms and Vacancies.

We compare the energies of different configurations corresponding to Ti atoms adsorbed on different sites of the 2D J-MoSSe surface to find stable configurations. The Ti adatoms will possibly migrate from one hollow site to another hollow site on the surface of 2D J-MoSSe during the preparation process. The migration barriers for Ti adatoms are 0.8 eV on the S surface (0.6 eV on the Se surface), as shown in Figure 3a. Interestingly, the hollow site ($Ti_S^{ad\text{-}h}$) is the most stable site for the Ti atom to be adsorbed on the S surface, while the Mo-top site ($Ti_{Se}^{ad\text{-}t}$) is the most stable site for the Ti atom to be adsorbed on the Se surface. These results motivate us to only

https://doi.org/10.1021/acs.jpcc.1c01918
J. Phys. Chem. C 2021, 125, 11939−11949

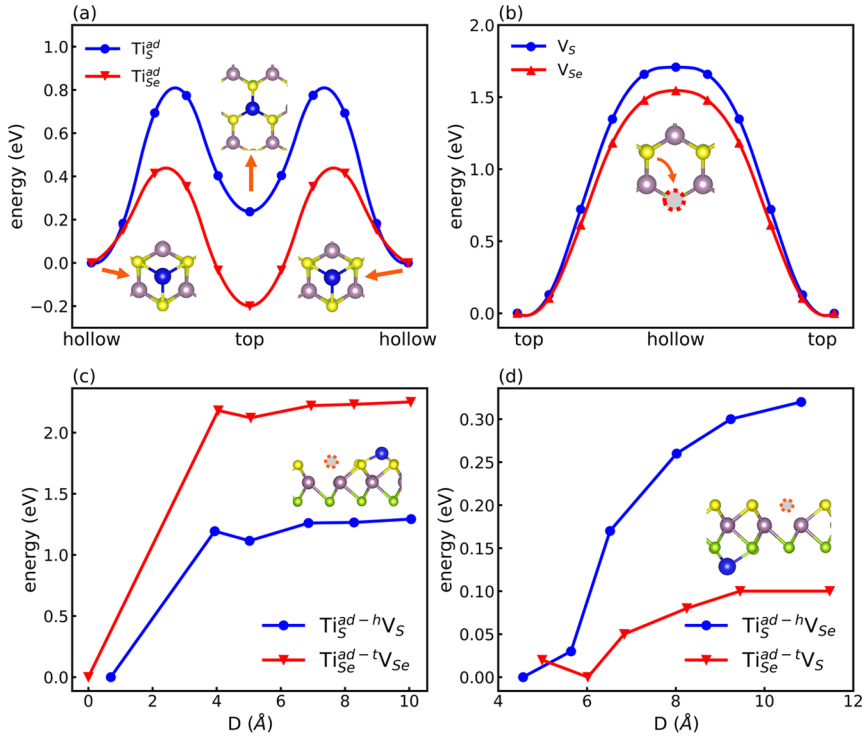

Figure 3. (a) Energy variation for adsorbed Ti atoms migrating from one hollow site to the adjacent hollow site by passing a middle Mo-top site. The energies are set to zero for adsorbed Ti atoms at the hollow site. (b) Energy variation for V_S and V_{Se} migrating from a top site to another top site by passing a hollow site. The energies are set to zero for S or Se atoms at the top site. (c) Relative energy of configurations varying with the distance (D) between Ti adatoms and S/Se vacancies coexisting on one surface of 2D J-MoSSe. (d) Relative energy varying with the distance between Ti adatoms and S/Se vacancies on both surfaces. The lowest energy is set to zero for each type of configuration.

consider the two adatom cases in subsequent exploration: $Ti_S^{ad\text{-}h}$ and $Ti_{Se}^{ad\text{-}t}$.

The vacancies on the surface of 2D J-MoSSe may migrate similarly to Ti adatoms. The migration of S or Se vacancies is identical to the exchange of S or Se atoms with the nearby vacancies, as shown in Figure 3b. We calculate the energy barriers as 1.7 or 1.5 eV for the migration of V_S or V_{Se}, respectively. The vacancies will diffuse only with difficulty after appearing on the surface. Our results show that migration barriers on the S side are larger than corresponding values on the Se side for both Ti adatoms and vacancies. We hypothesize that this is due to the larger electronegativity of sulfur, leading to stronger bonds with Ti and Mo atoms compared with selenium.

3.2. Interaction between the Coexisting Ti Atoms and Vacancies. As mentioned above, both the adsorbed Ti atoms and S/Se vacancies are difficult to migrate once these defects appear on the surface of 2D J-MoSSe. The adsorbed sites of Ti atoms may appear near or far from the vacancy site. The detailed variation of energy with respect to adatom/vacancy distances is valuable for us to develop better models for calculating photocatalytic properties. There would obviously be different energy scales when considering defects distributed on the two different S/Se surfaces. The combination of two defect sites weakens the lattice distortion and reduces the total energy. We systematically investigate the energy of various possible configurations of 2D J-MoSSe with different Ti adatom and vacancy locations. There are four cases—(1) the Ti adatom at the hollow site and the vacancy exist on the S surface ($Ti_S^{ad\text{-}h}V_S$), (2) the Ti adatom at the Mo-top site and the vacancy on the Se surface ($Ti_{Se}^{ad\text{-}t}V_{Se}$), (3) Ti at the hollow site on the S surface and vacancy on the Se surface ($Ti_S^{ad\text{-}h}V_{Se}$), and (4) Ti at the Mo-top site on the Se surface and the vacancy on the S surface ($Ti_{Se}^{ad\text{-}t}V_S$). In this work, the distance is defined as the variation of Ti adatoms adsorbed at different sites with respect to a S/Se vacancy, as shown in Figure S3.

In the simplest cases where the adatoms are located on the same surface as the vacancy, we find that the total energy decreases slightly as a Ti adatom get closer to a S/Se vacancy, as shown in Figure 3c. As the vacancy and Ti adatom become adjacent, the energy dramatically decreases by approximately 1 eV (2 eV). These results indicate that the vacancy traps the adsorbed Ti atom nearby because there is an effective attraction between the two types of defects. In these cases, the Ti adatom migrates to the vacancy site and transforms to a substituted Ti atom, as shown in Figure S3b.

For the defects on both surfaces, we first notice that the energy scale is dramatically different compared with the previous simplest cases. The total energy increases by about 0.1 eV (0.3 eV) for configurations of $Ti_S^{ad\text{-}h}V_{Se}$ ($Ti_{Se}^{ad\text{-}t}V_S$) as the distance increases. The vacancy obviously cannot trap the Ti adatom because the molybdenum layer separates the two defects. The energy increase of the $Ti_S^{ad\text{-}h}V_{Se}$ configuration (0.3 eV) is faster than that of the $Ti_{Se}^{ad\text{-}t}V_S$ configuration (0.1 eV), as shown in Figure 3d. A stronger bonding between the Ti adatom on the S surface leads to a stronger Coulomb attraction between the Ti adatom and the localized electron at the Se vacancy. This stronger Coulomb attraction induces a larger increase in total interaction energy compared with the pristine structure. The binding strength of $Ti_{Se}^{ad\text{-}t}V_S$ configuration is weaker compared with $Ti_S^{ad\text{-}h}V_{Se}$ because the Ti adatom binds more strongly to sulfur. There is a dip in the configuration of $Ti_{Se}^{ad\text{-}t}V_S$ as the distance increases from 5 to 6

https://doi.org/10.1021/acs.jpcc.1c01918
J. Phys. Chem. C 2021, 125, 11939−11949

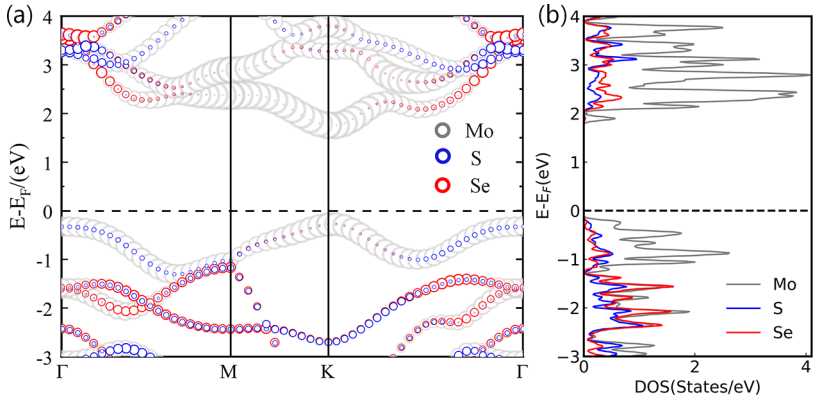

Figure 4. (a) Projected band structure and (b) density of states of pristine MoSSe calculated with the HSE06 functional.

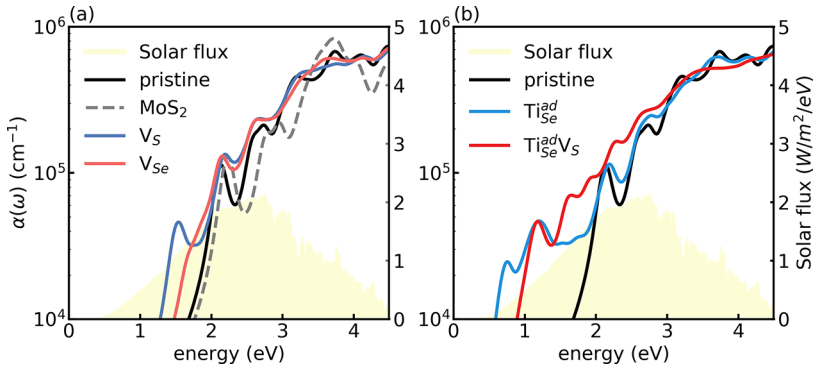

Figure 5. Optical absorption spectrum of pristine and defected 2D J-MoSSe. (a) Spectra of pristine 2D J-MoSSe, MoS_2, and MoSSe with S vacancy (V_S) and Se vacancy (V_{Se}). (b) Spectra of configurations containing adsorbed Ti atoms ($Ti_{Se}^{ad\text{-}t}$) and coexisting vacancies ($Ti_{Se}^{ad\text{-}t}V_S$). $TiSe^{ad}$ is the simplification of $Ti_{Se}^{ad\text{-}t}$ for convenience. The black curves in panels (a) and (b) show the spectrum of pristine MoSSe. The light-yellow shadows indicate the flux of solar radiation.[53]

Å, which may be caused by stronger Coulomb repulsion between Mo and the right-top Ti atom that induces the higher energy of the structure at 5 Å when the opposite nonmetal S atoms are removed, as shown in Figure S4.

These results generally demonstrate that vacancies will trap nearby Ti adatoms. Both the lattice distortions and Coulomb interactions affect the total energy of these adatom−vacancy configurations. Therefore, the adsorbed Ti atoms are more likely to distribute at sites adjacent to vacancies or even get trapped by the vacancies when they are on the same surface. A coexisting substituted Ti atom and vacancy on the 2D J-MoSSe surface may appear when there are excess vacancies (when the number of vacancies is greater than the number of Ti atoms). We find that the energy also decreases with decreasing distance between the substituted Ti atom and S/Se vacancy, as shown in Figure S5; these results are similar to what we found for the Ti adatoms and S/Se vacancies. Ti atoms (substituted or adatom) coexisting on the sites adjacent to S/Se vacancies will produce configurations with the lowest energies. These lowest-energy configurations are thereby thermodynamically favorable; we select these configurations to further our exploration of photocatalytic properties in the nonpristine 2D J-MoSSe system as shown in Figure S6.

3.3. Optical Absorption Spectra. The utilization of sunlight is a critical key for energy conversion in photocatalysis. The pristine MoSSe has a direct band gap of 2.04 eV, as shown in the projected band structure and density of states in Figure 4. The Mo d-states contribute the most to the conduction/valence band edges, and the S p-states contribute more to the valence band edges compared with the Se p-states, while the Se p-states contribute more to the conduction band edges. The calculated absorption range of pristine 2D J-MoSSe includes the sunlight region above the photon energy of 1.7 eV with the first absorption peak at about 2.1 eV, as shown in Figure 5a. The 2D J-MoSSe structure exhibits improved sunlight utilization compared with MoS_2, which is consistent with the published results.[30] Defects of Ti atoms (substituted and adatoms) and S/Se vacancies will introduce defect states, thereby extending the optical absorption range of 2D J-MoSSe materials. As a baseline for more complex configurations, we explore the properties of configurations with isolated Ti atoms or S/Se vacancies and use these results for comparison to the more complex configurations.

First, we find that vacancies, V_S or V_{Se}, will extend the calculated absorption limit to 1.3 or 1.5 eV, respectively, as shown in Figure 5a. The vacancies will also increase the absorption coefficients by filling valleys in the absorption spectra of pristine 2D J-MoSSe. Next, we find that the adsorbed Ti atoms on the Se-side surface dramatically extend the optical absorption limit by approximately 1 eV compared with the previously discussed pristine structures. This increased optical absorption will enable the absorption range to cover most of the visible region, as seen in Figure 5b. We also explored the optical absorption spectra varying with different concentrations of adsorbed Ti atoms. Moreover, the results show that a 3−8% ratio of adsorbed Ti atom has a remarkable enhancement and even a small doping ratio of 0.9% exhibits obvious improvement, as described in Figure S7.

https://doi.org/10.1021/acs.jpcc.1c01918
J. Phys. Chem. C 2021, 125, 11939−11949

Table 1. Electrostatic Potential Difference (ΔV) between the Two Surfaces for Pristine and Defected 2D J-MoSSe[a]

configuration	pristine	V_S	$Ti_S^{ad\text{-}h}$	$Ti_S^{ad\text{-}h}V_{Se}$	Ti_S	Ti_SV_S	Ti_SV_{Se}
ΔV (eV)	0.77	0.77	0.11	−0.17	0.24	0.26	0.19
configuration	V_{Se}	$Ti_{Se}^{ad\text{-}t}$	$Ti_{Se}^{ad\text{-}t}V_S$	Ti_{Se}	$Ti_{Se}V_{Se}$	$Ti_{Se}V_S$	
ΔV (eV)	0.73	1.66	1.71	1.11	1.05	1.12	

[a]The value of −0.17 eV indicates the reversed ΔV with direction contrary to the intrinsic potential difference in pristine 2D J-MoSSe.

Substituted Ti atoms (Ti_S and Ti_{Se}) only slightly extend the calculated optical absorption range to about 1.6 eV compared with the pristine 2D J-MoSSe. The optical spectra of defects existing alone demonstrate that Ti adatoms induce a broader optical absorption range than substituted Ti atoms and S/Se vacancies.

Of course, the S/Se vacancies are likely to coexist with either adsorbed or substituted Ti atoms on the surface of 2D J-MoSSe. So, now, we will discuss these more complex situations. The coexisting S vacancy in the $Ti_{Se}^{ad\text{-}t}V_s$ configuration narrows the optical absorption range to about 0.2 eV compared with the $Ti_{Se}^{ad\text{-}t}$ configuration, as shown in Figure 5b. The S vacancy further increases the absorption coefficient by filling valleys in the absorption spectra. The increased absorption coefficient mostly distributes at the energy range from 1.5 to 3 eV, which is ideal for photocatalytic water splitting because this energy range is in the region of higher-powered sunlight. The adsorbed Ti atom on the S-side surface ($Ti_S^{ad\text{-}h}$) shows similar performance, as shown in Figure S7c. For the configurations of vacancies coexisting with substituted Ti atoms (Ti_SV_S, Ti_SV_{Se}, $Ti_{Se}V_S$, and $Ti_{Se}V_{Se}$), we find that the coexisting S/Se vacancies further extend the calculated absorption limit to about 1.3 eV, as shown in Figure S7a,b. The coexisting S/Se vacancies also increase the optical absorption coefficients. These spectra illustrate that the S/Se vacancies coexisting with Ti adatoms obviously increase the optical absorption coefficients and improve the conversion efficiency of solar energy. The configuration of S/Se vacancies coexisting with substituted Ti atoms have only a moderately extended optical absorption range and increased absorption coefficient, which will also improve the conversion efficiency of solar energy.

Overall, the coexisting Ti adatoms and S/Se vacancies have the optimal synergistic effect on the harvest of sunlight when distributed on both surfaces of 2D J-MoSSe. We propose that the synergistic effects come from redistributed defect states when Ti adatoms and S/Se vacancies coexist. The unfolded band structures of pristine 2D MoSSe, $Ti_{Se}^{ad\text{-}t}$, V_S, and $Ti_{Se}^{ad\text{-}t}V_S$ present clear figures of the defect states, as shown in Figure S8. The S vacancy (V_S) by itself introduces shallower defect levels to the band structure as compared with the Ti adatom ($Ti_{Se}^{ad\text{-}t}$) by itself, as shown in Figure S8b,c. Our calculations of $Ti_{Se}^{ad\text{-}t}$ configurations demonstrate a broader optical absorption range compared with the calculations of configurations with S vacancy (V_S), as shown in Figure S8e. The first absorption peak at 0.6 eV corresponds to the transition of electrons from defect levels to the conduction band minimum (CBM).

In the more complex configurations (Ti adatoms coexisting with S vacancies, $Ti_{Se}^{ad\text{-}t}V_S$), our calculations demonstrate that the band structure exhibits more dispersive defect levels compared with the previously aforementioned simpler cases. The first absorption peak is located at 1.2 eV for $Ti_{Se}^{ad\text{-}t}V_S$, and this corresponds to the transition of electrons from the valence band maximum (VBM) to the shallow defect levels, as shown in Figure S8d. The S vacancy within the $Ti_{Se}^{ad\text{-}t}V_S$ configuration slightly narrows the optical absorption range compared with the $Ti_{Se}^{ad\text{-}t}$ configuration, as shown in Figure S8e. A slightly blue-shifted first absorption peak in the spectrum of the $Ti_{Se}^{ad\text{-}t}V_S$ optical absorption calculation indicates that the deep defect states would not trap the photogenerated electrons, thereby discouraging the charge carriers from transporting to the potential level of the redox reaction. Our calculations indicate similar results for the $Ti_S^{ad\text{-}h}V_{Se}$ configuration, as shown in Figure S7c, but the optical absorption range is narrower than the absorption range of $Ti_{Se}^{ad\text{-}t}V_S$. These results demonstrate that the properties of the $Ti_{Se}^{ad\text{-}t}V_S$ configuration exhibit optimal synergistic effects within the optical absorption spectrum, which are more suitable for both harvesting sunlight and encouraging photocatalysis.

3.4. Band Edges with Respect to the Redox Potentials of Water. The band edges of a photocatalyst should straddle the redox potentials of water splitting to enable the transition of electron−hole pairs from the conduction/valence bands to the redox potential levels. The pristine 2D J-MoSSe has a band gap of 2.04 eV as per our calculated results using the HSE06 functional, and our calculated CBM and VBM levels properly straddle the redox potentials, as shown in Figure 1a. For pristine 2D J-MoSSe, the calculated electrostatic potential difference (ΔV) is 0.77 eV, as shown in Table 1, consistent with reported results,[32] which will drive the photogenerated electrons and holes to distribute on the Se and S surfaces, respectively. Therefore, without defects, the band edges of pristine 2D J-MoSSe fulfill the requirements for photocatalysis. However, the CBM is too close to the reductive potential without being increased by ΔV. With the electrostatic potential difference, ΔV, added, the CBM and VBM levels bend upward along the direction of the internal electric field and the ΔV upshifts the CBM level and its density of states is located primarily on the Se side. The energy difference between CBM and the reductive potential increases and is comparable with the difference between the VBM and the oxidative potential level. The comparable energy difference will induce an analogous reaction rate between the hydrogen evolution reaction (HER) and oxygen evolution reaction (OER) and improve the overall efficiency.

The defects of S/Se vacancies and Ti atoms (substituted or adsorbed) will enhance or reduce the ΔV by different extents. Our calculations show that the intrinsic S or Se vacancies hardly change the ΔV compared with the pristine 2D J-MoSSe. Both adsorbed and substituted Ti atoms will increase the ΔV when distributing on the Se surface while decrease the ΔV when on the S surface. The Ti adatoms in the $Ti_{Se}^{ad\text{-}t}$ configuration increase the ΔV to 1.66 eV, while the Ti adatoms in the $Ti_S^{ad\text{-}h}$ configuration decrease the ΔV to 0.11 eV. These changes result from Ti ions existing as centers of positive charge as the outmost electrons of Ti atoms will transfer to S or Se atoms. These Ti ions with a positive charge will enhance the internal electric field of MoSSe pointing from

https://doi.org/10.1021/acs.jpcc.1c01918
J. Phys. Chem. C 2021, 125, 11939−11949

Se to S atom layers when the ions distribute on the Se surface while weaken the electric field when Ti ions distribute on the S surface, which is consistent with reported results.[29] The Ti adatom introduces a larger increase to ΔV than the substituted one. These results indicate that either adsorbed or substituted Ti atoms on the Se-side surface are more favorable to enhance the ΔV of 2D J-MoSSe.

The doped Ti atoms along with existing S/Se vacancies on the surface of 2D J-MoSSe will also adjust ΔV and will shift the band edges. The S vacancy tends to slightly increase ΔV, while the Se vacancy decreases ΔV a bit. The defects in $Ti_{Se}^{ad\text{-}t}V_S$ configuration induce a slightly larger ΔV of 1.71 eV compared with $Ti_{Se}^{ad\text{-}t}$. The results of ΔV indicate that only Ti atoms (substituted or adsorbed) on the S-side surface decrease the ΔV no matter if the Ti atoms exist alone or coexist with S/Se vacancies. There are no obvious changes for the CBM and VBM levels of configuration V_S, $Ti_{Se}^{ad\text{-}t}V_S$, and $Ti_{Se}^{ad\text{-}t}$ compared to the pristine 2D J-MoSSe, as shown in Figure S8. The band edges of these configurations still distribute on the Se and S surfaces, respectively, and CBM levels bend upward to straddle the redox potential levels of water-splitting reaction similarly to the pristine 2D J-MoSSe. The increased polarization of doped Ti atoms on the Se-side surface will reduce the exciton binding energy and promote the separation of photogenerated charge carriers, thereby increasing the solar-to-hydrogen conversion efficiency.[54]

3.5. Carrier Separation and Transport. The separation and transport of photoinduced carriers are another key steps for photocatalytic water splitting that greatly affect the efficiency of the redox reaction. The internal electric field not only shifts the band edges but also boosts the separation of electrons and holes in 2D J-MoSSe.[55] The charge carriers will separate more efficiently in the configurations with Ti atoms (adsorbed or substituted) on the Se surface because of the increased ΔV regardless of the Ti atom existing alone or coexisting with vacancies. The $Ti_{Se}^{ad\text{-}t}$ and $Ti_{Se}^{ad\text{-}t}V_S$ configurations will possess a higher efficiency for photocatalytic water splitting because the internal electric field is enhanced by the change in electrostatic potential difference, ΔV.

The effective mass dictates the transport efficiency of charge carriers. We study the effective mass from the curvature of the conduction/valence energy bands based on the unfolded band structures, as shown in Figure S9. From the carrier's effective mass shown in Figure 6, pristine 2D J-MoSSe has an effective carrier mass smaller than the free electron mass m_0 and exhibits very weak $x-y$ direction anisotropy and hole−electron asymmetry. For the defects existing alone, the vacancies (V_S and V_{Se}) have minor effects on the carrier effective mass. The Ti adatoms ($Ti_S^{ad\text{-}h}$ and $Ti_{Se}^{ad\text{-}t}$) also have little impact on the effective mass. The substituted Ti atoms (Ti_S and Ti_{Se}) severely increase the effective mass both of electrons and holes to about $2-3m_0$. The defect Ti_{Se} introduces distinct differences between the effective mass of electrons and holes, which will promote the separation of hole−electron pairs. The effective mass results of V_{Se} and $Ti_S^{ad\text{-}h}$ are shown in Figure S10. These effective mass results demonstrate that only substituted Ti atoms induce a large effective mass of charge carriers and yield decreases in the transport efficiency of charge carriers. The S/Se vacancies and Ti adatoms induce small changes in the effective mass of charge carriers, thereby having little impact on the efficient transporting of charge carriers in 2D J-MoSSe.

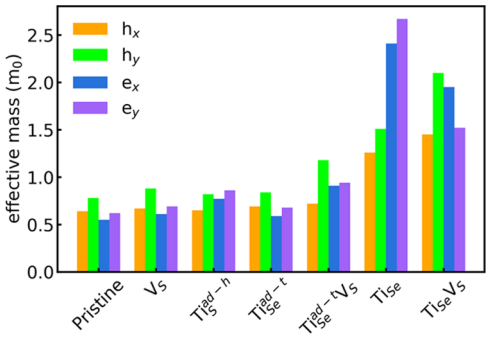

Figure 6. Effective masses of electrons and holes in pristine and defected 2D J-MoSSe. h_x, h_y and e_x, e_y denote the effective masses of holes and electrons in the x and y direction, respectively.

More factors contribute to the changes in the effective mass for systems where S/Se vacancies and Ti atoms (substituted or adsorbed) coexist, leading to complex interpretations. The S vacancies and Ti adatoms in the $Ti_{Se}^{ad\text{-}t}V_S$ configuration induce increases in the carrier mass. The effective mass of electrons slightly increases to about m_0 and exhibits a large $x-y$ direction anisotropy for the $Ti_{Se}^{ad\text{-}t}V_S$ configuration. The defects in the $Ti_S^{ad\text{-}h}V_{Se}$ configuration yield larger effective masses for electrons compared with those for holes, as shown in Figure S10, thereby promoting separation of electron−hole pairs. Substituted Ti atoms coexisting with S/Se vacancies in the Ti_SV_S, $Ti_{Se}V_{Se}$, Ti_SV_{Se}, and $Ti_{Se}V_S$ configurations have an obvious negative impact on the effective mass of charge carriers. The larger effective mass of the $Ti_{Se}V_S$ configuration exhibits an apparent $x-y$ direction anisotropy compared with the Ti adatom configurations ($Ti_{Se}^{ad\text{-}t}V_S$ and $Ti_S^{ad\text{-}h}V_{Se}$) because the substituted Ti atom coexisting with the S vacancy introduces a larger lattice distortion into the initial structure, thereby breaking the local symmetry of the 2D J-MoSSe structure. The broken local symmetry reduces the curvature and enhances the $x-y$ direction anisotropy of conduction/valence bands, as shown in Figure S9f. The defects containing Ti adatoms with S/Se vacancies only slightly increase the effective mass of charge carriers, while the defects containing substituted Ti atoms increase the effective mass and reduce the transport efficiency of photogenerated electrons and holes.

3.6. Surface Catalytic Reaction. The hydrogen evolution reaction (HER) is the last step for hydrogen generation in photocatalytic water splitting. The reaction barrier for reducing the hydrogen ion is determined by the free energy (ΔG_{H^*}) and characterizes the reaction rate for HER. There are multiple active sites in doped 2D J-MoSSe for the adsorption of hydrogen atoms including S/Se vacancy sites and Ti top sites. The ΔG_{H^*} barriers of pristine 2D J-MoSSe are too high, yielding very poor performance to catalyze HER, as shown in Figure S11. For isolated defects, the S/Se vacancies in the V_S and V_{Se} configurations decrease the barrier ΔG_{H^*} to −0.1 and 0.01 eV, respectively, as shown in Figure 7, and these ΔG_{H^*} values imply excellent catalytic activity, which is consistent with the experimental results.[28] The adsorption energy of H atoms on these vacancy sites is approximate −0.2 eV, which is quite lower than the adsorption energy on the pristine 2D J-MoSSe surface (1.61 eV), as shown in Figure S11. The adsorption of H atoms on vacancy sites is quite stable, and the H atoms require large energy to migrate to another surface site on the pristine surface. The Ti adatom in the $Ti_S^{ad\text{-}h}$ configuration also induces near-zero ΔG_{H^*} values similar to the configurations containing only S/Se vacancies. The Ti

https://doi.org/10.1021/acs.jpcc.1c01918
J. Phys. Chem. C 2021, 125, 11939−11949

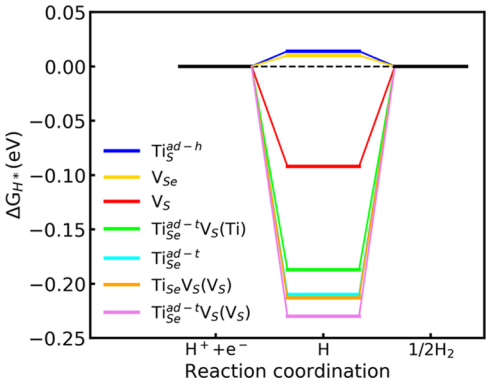

Figure 7. Change of Gibbs free energy (ΔG_{H^*}) for HER on vacancy or Ti top sites of defected 2D J-MoSSe. $Ti_{Se}^{ad\text{-}t}V_S$ (Ti) means the Ti top site, and $Ti_{Se}^{ad\text{-}t}V_S$ (V_S) means the vacancy site in configuration $Ti_{Se}^{ad\text{-}t}V_S$. The sites are HER-active with ΔG_{H^*} between −0.2 and 0.2 eV.

adatoms in the $Ti_{Se}^{ad\text{-}t}$ configuration induce a ΔG_{H^*} of approximately −0.2 eV, which is still appropriate for catalyzing HER.[34,56,57] In contrast, substitutional Ti atoms within the Ti_S and Ti_{Se} configurations induce larger ΔG_{H^*} values of approximately 0.9 eV, as shown in Figure S11.

Now, we consider the very complex configurations containing both S/Se vacancies and Ti atoms (either substitutional or adatoms). The defects in the $Ti_{Se}^{ad\text{-}t}V_S$ configuration also induce moderate changes in the ΔG_{H^*} barriers compared with the Ti top site of the $Ti_{Se}^{ad\text{-}t}$ configuration without vacancies. The ΔG_{H^*} values of vacancy sites within the Ti_SV_S, $Ti_{Se}V_S$, and Ti_SV_{Se} configurations are approximately −0.1 eV, as shown in Figure S11. These vacancy sites are also HER-active. From the free energy values discussed above, the vacancy and Ti adatom top sites are generally the most catalytically active sites for HER, while the substituted Ti atoms will not improve the HER catalytic efficiency.

The catalytic efficiency for OER determines the draining efficiency of photogenerated holes. The accumulated holes in the valence band will recombine with the excited electrons within 2D J-MoSSe, which will decrease the efficiency of HER. We explore the reaction barrier of OER for the promising defect discussed above, as shown in Figure S12. The energy difference between VBM and the hydrogen reduction potential supplies external potential for the holes to overcome the energy barriers along the OER pathway.[19] The energy barrier on the pristine S-side surface is 0.46 eV for OER, so the S-side surface will not catalyze OER in a high efficiency, which is consistent with the previous work.[58] The reaction barriers on the V_S site, Ti_S site, $Ti_S^{ad\text{-}h}$ site, and V_S site in $Ti_{Se}^{ad\text{-}t}V_S$ are even higher. We deduce that the strong bonding between these reaction sites and oxygen atom is accountable for the high energy barrier. Although the defect sites of Ti doping and S vacancies will not fulfill the requirement of OER, Ti-doped MoSSe with vacancies will catalyze HER as an anode in a photoelectrochemical cell. There are novel OER catalysts with high efficiency in catalyzing OER, which act as a promising cathode in the cell. For example, Ni-doped MoSSe will catalyze OER efficiently from the calculated results.[59] Cobalt oxide with oxygen vacancy is also an efficient OER catalyst as verified by the experimental results.[60]

4. CONCLUSIONS

The properties of configurations above should meet as many requirements mentioned above as possible for photocatalytic reaction with a series of steps. The rules we take for selecting optimal configurations are as follows: first, the defects should not weaken the internal electric field greatly; second, these defects should improve the optical absorption properties by either extending the optical absorption range or increasing the absorption coefficient; third, the structure should contain active sites for HER; last, the charge carriers should separate efficiently and transfer quickly to the reaction sites. Although Ti adatoms in the $Ti_S^{ad\text{-}h}$ configuration extend the optical absorption range and decrease ΔG_{H^*} values very close to zero, the Ti atom reduces the ΔV from 0.77 to 0.1 eV, which diminishes the main advantage of 2D J-MoSSe. So, the Ti adatoms on the Se surface are superior. The coexisting defects in $Ti_{Se}^{ad\text{-}t}V_S$ configuration increase the ΔV to 1.7 eV, extend the optical absorption limit of 0.9 eV, increase the absorption coefficient, and decrease the hydrogen adsorption free energy barrier to −0.19 eV. The configuration $Ti_{Se}^{ad\text{-}t}V_S$ is more promising in photocatalytic water splitting than the reported 2D Janus WSSe because the optical absorption limit of 2D Janus WSSe is approximate 2.0 eV,[26] the ΔV is 0.73 eV, and the energy barrier for HER is 0.58 eV.[19] These indexes indicate a lower solar-to-hydrogen energy conversion efficiency compared with that of the $Ti_{Se}^{ad\text{-}t}V_S$ configuration. We predict that this $Ti_{Se}^{ad\text{-}t}V_S$ configuration exhibits the best overall photocatalytic performance among all of the configurations we had considered. The $Ti_S^{ad\text{-}h}$ and V_{Se} configurations also look promising based on the similar properties aforementioned. Substituted Ti atoms show less likelihood of photocatalytic activity, and we propose that these systems should be avoided. If one hopes to obtain improved photocatalytic applications, then one should also prepare materials with few vacancies, particularly, on the Se surface. However, Ti adatoms deposited on the Se surface will transform to the $Ti_{Se}^{ad\text{-}t}V_S$ configuration if there are S vacancies that will produce a promising photocatalytic material.

In conclusion, we have demonstrated by systematically exploring the structures and properties of 2D J-MoSSe (with Ti doping and S/Se vacancies) that there are synergistic effects on photocatalytic activity. Both adsorbed Ti atoms and S or Se vacancies cannot migrate on the surface once appearing given the high energy barrier. The doped Ti atoms energetically prefer sites adjacent to vacancies. Adsorbed Ti atoms enlarge the range of optical absorption dramatically, and coexisting vacancies will further increase the absorption coefficient. Overall, Ti atoms will strengthen the internal electric field only when adsorbing on the Se side. The vacancy site and top site of adsorbed Ti atom are generally HER catalytically active with hydrogen adsorption free energies in the range from −0.2 to 0.2 eV. The defects in $Ti_{Se}^{ad\text{-}t}V_S$ configuration exhibit the most synergistic effects on the improvement of the optical absorption spectrum and internal electric field, which induce better overall photocatalytic activity by taking the above factors into account.

■ ASSOCIATED CONTENT

Supporting Information

The Supporting Information is available free of charge at https://pubs.acs.org/doi/10.1021/acs.jpcc.1c01918.

https://doi.org/10.1021/acs.jpcc.1c01918
J. Phys. Chem. C 2021, 125, 11939−11949

Structures of MoS_2 and MoSSe, structure of doped 2D J-MoSSe, definition of the distance, variation of energy with distance, low-energy structures, optical absorption spectra, unfolded band structures, projected density of states, effective mass, hydrogen adsorption energy and free energy, and variation of free energy along the OER pathway (PDF)

AUTHOR INFORMATION

Corresponding Authors

James P. Lewis − *State Key Laboratory of Coal Conversion, Institute of Coal Chemistry, Chinese Academy of Sciences, Taiyuan, Shanxi 030001, China; Beijing Advanced Innovation Center for Materials Genome Engineering, Beijing Information S&T University, Beijing 101400, China;* orcid.org/0000-0002-6724-3483; Email: james.p.lewis.phd@gmail.com

Qing-Bo Yan − *Center of Materials Science and Optoelectronics Engineering, College of Materials Science and Opto-Electronic Technology, University of Chinese Academy of Sciences, Beijing 100049, China;* orcid.org/0000-0002-1001-1390; Email: yan@ucas.ac.cn

Gang Su − *Center of Materials Science and Optoelectronics Engineering, College of Materials Science and Opto-Electronic Technology, University of Chinese Academy of Sciences, Beijing 100049, China; School of Physical Sciences, University of Chinese Academy of Sciences, Beijing 100049, China; Kavli Institute for Theoretical Sciences, and CAS Center of Excellence in Topological Quantum Computation, University of Chinese Academy of Sciences, Beijing 100190, China*; Email: gsu@ucas.ac.cn

Authors

Yi-Ming Zhao − *Center of Materials Science and Optoelectronics Engineering, College of Materials Science and Opto-Electronic Technology, University of Chinese Academy of Sciences, Beijing 100049, China;* orcid.org/0000-0002-3921-1900

Pengju Ren − *State Key Laboratory of Coal Conversion, Institute of Coal Chemistry, Chinese Academy of Sciences, Taiyuan, Shanxi 030001, China;* orcid.org/0000-0003-3752-1638

Xing-Yu Ma − *School of Physical Sciences, University of Chinese Academy of Sciences, Beijing 100049, China;* orcid.org/0000-0001-5268-5169

Complete contact information is available at: https://pubs.acs.org/10.1021/acs.jpcc.1c01918

Notes

The authors declare no competing financial interest.

ACKNOWLEDGMENTS

This work is supported in part by the National Key R&D Program of China (Grant No. 2018YFA0305800), the Strategic Priority Research Program of CAS (Grant No. XDB28000000), the NSFC (Grant No. 11834014), and Beijing Municipal Science and Technology Commission (Grant No. Z118100004218001); J.P.L. received support from the Thousand Talent program of the Chinese Academy of Sciences and Fundamental Research Funds for the Central Universities. The authors thank Prof Zheng-Chuan Wang, Prof Zhen-Gang Zhu, Prof Bo Gu, Yurong He, Zhongxian Qiu, and Kuan-Rong Hao for valuable discussion.

ABBREVIATIONS

2D J-MoSSe, two-dimensional Janus MoSSe; CVD, chemical vapor deposition; CBM, conduction band minimum; VBM, valence band maximum; HER, hydrogen evolution reaction; OER, oxygen evolution reaction

REFERENCES

(1) Fu, C. F.; Wu, X.; Yang, J. Material Design for Photocatalytic Water Splitting from a Theoretical Perspective. *Adv. Mater.* **2018**, *30*, No. e1802106.

(2) Fujishima, A.; Honda, K. Electrochemical photolysis of water at a semiconductor electrode. *Nature* **1972**, *238*, 37−38.

(3) Guo, Q.; Zhou, C.; Ma, Z.; Yang, X. Fundamentals of TiO_2 Photocatalysis: Concepts, Mechanisms, and Challenges. *Adv. Mater.* **2019**, *31*, No. e1901997.

(4) Cheng, L.; Xiang, Q. J.; Liao, Y. L.; Zhang, H. W. CdS-Based photocatalysts. *Energy Environ. Sci.* **2018**, *11*, 1362−1391.

(5) Hou, Y.; Zheng, C.; Zhu, Z.; Wang, X. Microwave-assisted fabrication of porous hematite photoanodes for efficient solar water splitting. *Chem. Commun.* **2016**, *52*, 6888−6891.

(6) Tamirat, A. G.; Rick, J.; Dubale, A. A.; Su, W. N.; Hwang, B. J. Using hematite for photoelectrochemical water splitting: a review of current progress and challenges. *Nanoscale Horiz.* **2016**, *1*, 243−267.

(7) Hara, M.; Hitoki, G.; Takata, T.; Kondo, J. N.; Kobayashi, H.; Domen, K. TaON and Ta_3N_5 as new visible light driven photocatalysts. *Catal. Today* **2003**, *78*, 555−560.

(8) Fang, Y.; Zheng, Y.; Fang, T.; Chen, Y.; Zhu, Y.; Liang, Q.; Sheng, H.; Li, Z.; Chen, C.; Wang, X. Photocatalysis: an overview of recent developments and technological advancements. *Sci. China: Chem.* **2020**, *63*, 149−181.

(9) Chu, S.; Kong, X.; Vanka, S.; Guo, H.; Mi, Z. Artificial Photosynthesis on III-Nitride Nanowire Arrays. In *Semiconductors and Semimetals*; Mi, Z.; Wang, L.; Jagadish, C., Eds.; Elsevier, 2017; Chapter 6, Vol. *97*, pp 223−255.

(10) Li, R.; Li, C. Photocatalytic Water Splitting on Semiconductor-Based Photocatalysts. In *Advances in Catalysis*; Song, C., Ed.; Academic Press, 2017; Chapter 1, Vol. *60*, pp 1−57.

(11) Li, Y.; Gao, C.; Long, R.; Xiong, Y. Photocatalyst design based on two-dimensional materials. *Mater. Today Chem.* **2019**, *11*, 197−216.

(12) Singh, A. K.; Mathew, K.; Zhuang, H. L.; Hennig, R. G. Computational Screening of 2D Materials for Photocatalysis. *J. Phys. Chem. Lett.* **2015**, *6*, 1087−1098.

(13) Li, Y.; Li, Y.-L.; Araujo, C. M.; Luo, W.; Ahuja, R. Single-layer MoS_2 as an efficient photocatalyst. *Catal. Sci. Technol.* **2013**, *3*, 2214−2220.

(14) Parzinger, E.; Miller, B.; Blaschke, B.; Garrido, J. A.; Ager, J. W.; Holleitner, A.; Wurstbauer, U. Photocatalytic Stability of Single- and Few-Layer MoS_2. *ACS Nano* **2015**, *9*, 11302−11309.

(15) Splendiani, A.; Sun, L.; Zhang, Y.; Li, T.; Kim, J.; Chim, C. Y.; Galli, G.; Wang, F. Emerging photoluminescence in monolayer MoS_2. *Nano Lett.* **2010**, *10*, 1271−1275.

(16) He, Z.; Que, W. Molybdenum disulfide nanomaterials: Structures, properties, synthesis and recent progress on hydrogen evolution reaction. *Appl. Mater. Today* **2016**, *3*, 23−56.

(17) Li, Z.; Meng, X.; Zhang, Z. Recent development on MoS_2-based photocatalysis: A review. *J. Photochem. Photobiol., C* **2018**, *35*, 39−55.

(18) Wu, C.; Zhang, J.; Tong, X.; Yu, P.; Xu, J.-Y.; Wu, J.; Wang, Z. M.; Lou, J.; Chueh, Y.-L. A Critical Review on Enhancement of Photocatalytic Hydrogen Production by Molybdenum Disulfide: From Growth to Interfacial Activities. *Small* **2019**, *15*, No. 1900578.

(19) Ju, L.; Bie, M.; Tang, X.; Shang, J.; Kou, L. Janus WSSe Monolayer: An Excellent Photocatalyst for Overall Water Splitting. *ACS Appl. Mater. Interfaces* **2020**, *12*, 29335−29343.

(20) Peng, R.; Ma, Y.; Huang, B.; Dai, Y. Two-dimensional Janus PtSSe for photocatalytic water splitting under the visible or infrared light. *J. Mater. Chem. A* **2019**, *7*, 603−610.
(21) Ahammed, R.; Jena, N.; Rawat, A.; Mohanta, M. K.; Dimple; De Sarkar, A. Ultrahigh Out-of-Plane Piezoelectricity Meets Giant Rashba Effect in 2D Janus Monolayers and Bilayers of Group IV Transition-Metal Trichalcogenides. *J. Phys. Chem. C* **2020**, *124*, 21250−21260.
(22) Bai, Y.; Zhang, Q.; Xu, N.; Deng, K.; Kan, E. The Janus structures of group-III chalcogenide monolayers as promising photocatalysts for water splitting. *Appl. Surf. Sci.* **2019**, *478*, 522−531.
(23) Rawat, A.; Ahammed, R.; Dimple; Jena, N.; Mohanta, M. K.; De Sarkar, A. Solar Energy Harvesting in Type II van der Waals Heterostructures of Semiconducting Group III Monochalcogenide Monolayers. *J. Phys. Chem. C* **2019**, *123*, 12666−12675.
(24) Nandi, P.; Rawat, A.; Ahammed, R.; Jena, N.; De Sarkar, A. Group-IV(A) Janus dichalcogenide monolayers and their interfaces straddle gigantic shear and in-plane piezoelectricity. *Nanoscale* **2021**, *13*, 5460−5478.
(25) Guo, Y.; Zhou, S.; Bai, Y.; Zhao, J. Enhanced piezoelectric effect in Janus group-III chalcogenide monolayers. *Appl. Phys. Lett.* **2017**, *110*, No. 163102.
(26) Xia, C.; Xiong, W.; Du, J.; Wang, T.; Peng, Y.; Li, J. Universality of electronic characteristics and photocatalyst applications in the two-dimensional Janus transition metal dichalcogenides. *Phys. Rev. B* **2018**, *98*, No. 165424.
(27) Lu, A. Y.; Zhu, H.; Xiao, J.; Chuu, C. P.; Han, Y.; Chiu, M. H.; Cheng, C. C.; Yang, C. W.; Wei, K. H.; Yang, Y.; et al. Janus monolayers of transition metal dichalcogenides. *Nat. Nanotechnol.* **2017**, *12*, 744−749.
(28) Zhang, J.; Jia, S.; Kholmanov, I.; Dong, L.; Er, D.; Chen, W.; Guo, H.; Jin, Z.; Shenoy, V. B.; Shi, L.; et al. Janus Monolayer Transition-Metal Dichalcogenides. *ACS Nano* **2017**, *11*, 8192−8198.
(29) Tao, S.; Xu, B.; Shi, J.; Zhong, S.; Lei, X.; Liu, G.; Wu, M. Tunable Dipole Moment in Janus Single-Layer MoSSe via Transition-Metal Atom Adsorption. *J. Phys. Chem. C* **2019**, *123*, 9059−9065.
(30) Guan, Z.; Ni, S.; Hu, S. Tunable Electronic and Optical Properties of Monolayer and Multilayer Janus MoSSe as a Photocatalyst for Solar Water Splitting: A First-Principles Study. *J. Phys. Chem. C* **2018**, *122*, 6209−6216.
(31) Li, X.; Li, Z.; Yang, J. Proposed photosynthesis method for producing hydrogen from dissociated water molecules using incident near-infrared light. *Phys. Rev. Lett.* **2014**, *112*, No. 018301.
(32) Ji, Y.; Yang, M.; Lin, H.; Hou, T.; Wang, L.; Li, Y.; Lee, S.-T. Janus Structures of Transition Metal Dichalcogenides as the Heterojunction Photocatalysts for Water Splitting. *J. Phys. Chem. C* **2018**, *122*, 3123−3129.
(33) Xu, Y.; Yao, Y.; Yin, W.; Cao, J.; Chen, M.; Wei, X. Intrinsic defect engineered Janus MoSSe sheet as a promising photocatalyst for water splitting. *RSC Adv.* **2020**, *10*, 10816−10825.
(34) Shi, W.; Li, G.; Wang, Z. Triggering Catalytic Active Sites for Hydrogen Evolution Reaction by Intrinsic Defects in Janus Monolayer MoSSe. *J. Phys. Chem. C* **2019**, *123*, 12261−12267.
(35) Hong, J.; Hu, Z.; Probert, M.; Li, K.; Lv, D.; Yang, X.; Gu, L.; Mao, N.; Feng, Q.; Xie, L.; et al. Exploring atomic defects in molybdenum disulphide monolayers. *Nat. Commun.* **2015**, *6*, No. 6293.
(36) Zhou, W.; Zou, X.; Najmaei, S.; Liu, Z.; Shi, Y.; Kong, J.; Lou, J.; Ajayan, P. M.; Yakobson, B. I.; Idrobo, J. C. Intrinsic structural defects in monolayer molybdenum disulfide. *Nano Lett.* **2013**, *13*, 2615−2622.
(37) Ma, X.; Yong, X.; Jian, C.-c.; Zhang, J. Transition Metal-Functionalized Janus MoSSe Monolayer: A Magnetic and Efficient Single-Atom Photocatalyst for Water-Splitting Applications. *J. Phys. Chem. C* **2019**, *123*, 18347−18354.
(38) Maschmeyer, T.; Rey, F.; Sankar, G.; Thomas, J. M. Heterogeneous catalysts obtained by grafting metallocene complexes onto mesoporous silica. *Nature* **1995**, *378*, 159−162.
(39) Durgun, E.; Dag, S.; Ciraci, S.; Gülseren, O. Energetics and Electronic Structures of Individual Atoms Adsorbed on Carbon Nanotubes. *J. Phys. Chem. B* **2004**, *108*, 575−582.
(40) Song, E.; Zhu, Y. Titanium Decorated Graphene as CO Detection Sensor. *Nanosci. Nanotechnol. Lett.* **2013**, *5*, 198−203.
(41) Liang, S.; Zhu, C.; Zhang, N.; Zhang, S.; Qiao, B.; Liu, H.; Liu, X.; Liu, Z.; Song, X.; Zhang, H.; et al. A Novel Single-Atom Electrocatalyst Ti_1/rGO for Efficient Cathodic Reduction in Hybrid Photovoltaics. *Adv. Mater.* **2020**, *32*, No. 2000478.
(42) Wang, L.; Lee, K.; Sun, Y.-Y.; Lucking, M.; Chen, Z.; Zhao, J. J.; Zhang, S. B. Graphene Oxide as an Ideal Substrate for Hydrogen Storage. *ACS Nano* **2009**, *3*, 2995−3000.
(43) Liao, J.-H.; Zhao, Y.-J.; Yang, X.-B. Controllable hydrogen adsorption and desorption by strain modulation on Ti decorated defective graphene. *Int. J. Hydrogen Energy* **2015**, *40*, 12063−12071.
(44) Ku, W.; Berlijn, T.; Lee, C.-C. Unfolding First-Principles Band Structures. *Phys. Rev. Lett.* **2010**, *104*, No. 216401.
(45) Medeiros, P. V. C.; Stafström, S.; Björk, J. Effects of extrinsic and intrinsic perturbations on the electronic structure of graphene: Retaining an effective primitive cell band structure by band unfolding. *Phys. Rev. B* **2014**, *89*, No. 041407.
(46) Giannozzi, P.; Andreussi, O.; Brumme, T.; Bunau, O.; Buongiorno Nardelli, M.; Calandra, M.; Car, R.; Cavazzoni, C.; Ceresoli, D.; Cococcioni, M.; et al. Advanced capabilities for materials modelling with Quantum ESPRESSO. *J. Phys.: Condens. Matter* **2017**, *29*, No. 465901.
(47) Kresse, G.; Furthmuller, J. Efficient iterative schemes for ab initio total-energy calculations using a plane-wave basis set. *Phys. Rev. B* **1996**, *54*, 11169−11186.
(48) Blöchl, P. E. Projector augmented-wave method. *Phys. Rev. B* **1994**, *50*, 17953−17979.
(49) Henkelman, G.; Uberuaga, B. P.; Jónsson, H. A climbing image nudged elastic band method for finding saddle points and minimum energy paths. *J. Chem. Phys.* **2000**, *113*, 9901−9904.
(50) Medeiros, P. V. C.; Tsirkin, S. S.; Stafström, S.; Björk, J. Unfolding spinor wave functions and expectation values of general operators: Introducing the unfolding-density operator. *Phys. Rev. B* **2015**, *91*, No. 041116.
(51) Hjorth Larsen, A.; Jorgen Mortensen, J.; Blomqvist, J.; Castelli, I. E.; Christensen, R.; Dulak, M.; Friis, J.; Groves, M. N.; Hammer, B.; Hargus, C.; et al. The atomic simulation environment-a Python library for working with atoms. *J. Phys.: Condens. Matter* **2017**, *29*, No. 273002.
(52) Wang, V.; Xu, N.; Liu, J. C.; Tang, G.; Geng, W.-T. VASPKIT: A User-friendly Interface Facilitating High-throughput Computing and Analysis Using VASP Code. 2019, arXiv:1908.08269. arXiv.org e-Print archive. http://arxiv.org/abs/1908.08269.
(53) Reference Solar Spectral Irradiance: Air Mass 1.5. http://rredc.nrel.gov/solar/spectra/am1.5 (accessed Oct 6, 2020).
(54) Ju, L.; Shang, J.; Tang, X.; Kou, L. Tunable Photocatalytic Water Splitting by the Ferroelectric Switch in a 2D $AgBiP_2Se_6$ Monolayer. *J. Am. Chem. Soc.* **2020**, *142*, 1492−1500.
(55) Ma, X.; Wu, X.; Wang, H.; Wang, Y. A Janus MoSSe monolayer: a potential wide solar-spectrum water-splitting photocatalyst with a low carrier recombination rate. *J. Mater. Chem. A* **2018**, *6*, 2295−2301.
(56) Nørskov, J. K.; Bligaard, T.; Logadottir, A.; Kitchin, J. R.; Chen, J. G.; Pandelov, S.; Stimming, U. Trends in the Exchange Current for Hydrogen Evolution. *J. Electrochem. Soc.* **2005**, *152*, No. J23.
(57) Hinnemann, B.; Moses, P. G.; Bonde, J.; Jorgensen, K. P.; Nielsen, J. H.; Horch, S.; Chorkendorff, I.; Norskov, J. K. Biomimetic hydrogen evolution: MoS_2 nanoparticles as catalyst for hydrogen evolution. *J. Am. Chem. Soc.* **2005**, *127*, 5308−5309.
(58) Zhao, F.; Li, J.; Chen, Y.; Zhang, M.; Zhang, H. Photocatalytic activity of co-doped Janus monolayer MoSSe for solar water splitting: A computational investigation. *Appl. Surf. Sci.* **2021**, *544*, No. 148741.
(59) Wu, Q.; Ma, Y.; Wang, H.; Zhang, S.; Huang, B.; Dai, Y. Trifunctional Electrocatalysts with High Efficiency for the Oxygen Reduction Reaction, Oxygen Evolution Reaction, and Na-O_2 Battery

https://doi.org/10.1021/acs.jpcc.1c01918
J. Phys. Chem. C 2021, 125, 11939−11949

in Heteroatom-Doped Janus Monolayer MoSSe. *ACS Appl. Mater. Interfaces* **2020**, *12*, 24066−24073.
(60) Ling, T.; Yan, D. Y.; Jiao, Y.; Wang, H.; Zheng, Y.; Zheng, X.; Mao, J.; Du, X. W.; Hu, Z.; Jaroniec, M.; et al. Engineering surface atomic structure of single-crystal cobalt (II) oxide nanorods for superior electrocatalysis. *Nat. Commun.* **2016**, *7*, No. 12876.

https://doi.org/10.1021/acs.jpcc.1c01918
J. Phys. Chem. C 2021, 125, 11939−11949